

PAPER • OPEN ACCESS

Electron diffraction by vacuum fluctuations

To cite this article: Valerio Di Giulio and F Javier García de Abajo 2020 *New J. Phys.* **22** 103057

View the [article online](#) for updates and enhancements.

You may also like

- [Demystifying the nonlocality problem in Aharonov–Bohm effect](#)
Kolahal Bhattacharya
- [Effects of anomalous magnetic moment in the quantum motion of neutral particle in magnetic and electric fields produced by a linear source in a conical spacetime](#)
Eugenio R. Bezerra de Mello
- [Optical Aharonov–Bohm effect due to toroidal moment inspired by general relativity](#)
A Besharat, M Miri and M Nouri-Zonoz

Recent citations

- [Optical Excitations with Electron Beams: Challenges and Opportunities](#)
F. Javier García de Abajo and Valerio Di Giulio
- [Modulation of Cathodoluminescence Emission by Interference with External Light](#)
Valerio Di Giulio *et al*



PAPER

Electron diffraction by vacuum fluctuations

OPEN ACCESS

RECEIVED
8 July 2020REVISED
28 September 2020ACCEPTED FOR PUBLICATION
2 October 2020PUBLISHED
29 October 2020

Original content from
this work may be used
under the terms of the
[Creative Commons
Attribution 4.0 licence](#).

Any further distribution
of this work must
maintain attribution to
the author(s) and the
title of the work, journal
citation and DOI.

Valerio Di Giulio^{1,*} and F Javier García de Abajo^{1,2,*} ¹ ICFO-Institut de Ciències Fòtoniques, The Barcelona Institute of Science and Technology, 08860 Castelldefels (Barcelona), Spain² ICREA-Institució Catalana de Recerca i Estudis Avançats, Passeig Lluís Companys 23, 08010 Barcelona, Spain

* Author to whom any correspondence should be addressed.

E-mail: valerio.digiulio@icfo.eu and javier.garciadeabajo@nanophotonics.es**Keywords:** electron microscopy, vacuum fluctuations, photonic nanostructures, light–matter interaction

Abstract

Vacuum fluctuations are known to produce electron diffraction leading to decoherence and self-interference. These effects have so far been studied as either an extension of the Aharonov–Bohm effect in front of a planar perfect conductor or through path integral analysis. Here, we present a simpler, general, and rigorous derivation based on a direct solution of the quantum electrodynamic loop interaction between the electron and a material structure in the temporal gauge. Our approach allows us to study dissipative media, for which we show examples of electron wave function shaping due to the interaction with real-metal surfaces. We further present a proof of the relation between the phase associated with vacuum fluctuations and the Aharonov–Bohm effect produced by the image self-interaction that is valid for arbitrary geometries. Besides their fundamental interest, our results could be useful for on-demand patterning of electron beams with potential application in nondestructive nanoscale imaging and spectroscopy.

1. Introduction

On-demand coherent manipulation of the transverse electron wave function in electron beams is of fundamental interest to improve spatial resolution in transmission electron microscopes. The problem can be simply stated as the question of how to introduce a position-dependent phase in the electron wave function. Currently, energetic electron beams can be focused down to sub-Ångström spots by phase shaping their transverse wave functions using electrostatic and magnetostatic lenses, which produce macroscopic changes in the phase profile to correct aberrations in the electron optics. Recently, perforated transmission phase plates have been successfully demonstrated to create beams carrying high values of angular momentum [1], while dynamical phase patterning has been explored with the use of pixelated electrostatic plates [2]. An alternative possibility consists in exploiting photon–electron interactions, which can affect the transversal phase as demonstrated for example in the Kapitza–Dirac effect [3, 4], and also in the recently demonstrated angular momentum transfer between light and electron beams [5]. This approach has been theoretically proposed to be useful for aberration correction [6], although it involves the emission or absorption of real photons, therefore producing inelastic rather than elastic diffraction.

In a related context, vacuum fluctuations can also induce a phase modulation without the exchange of real photons, an effect that has been theoretically investigated in the presence of nondissipative media [7] and is still lacking experimental confirmation to the best of our knowledge. For an electron moving parallel to a perfect conductor surface, this phase has been explained as arising from the Aharonov–Bohm effect [8] produced by the electron image potential [7], while an alternative derivation has been given in terms of path integrals [9]. The presence of material excitations with which the electron may interact could add new degrees of freedom to manipulate the quantum phase, although their study would be difficult to undertake using existing theoretical approaches. It should be noted that the same type of electron phase was analyzed in detail in early pioneering works in a different context related to electron microscopy and the understanding of elastic scattering by atomic crystal lattices for penetrating trajectories [10, 11]. However, the real part of the correction to the optical potential computed in these works was found to be too small in

samples with thickness smaller than the electron mean free path, and therefore, never experimentally observed as far as we know. In this context, aloof trajectories may enormously increase the interaction length, thus making this effect observable in practice.

In this work, we present an alternative derivation of vacuum phases produced during the interaction of electron beams with arbitrarily structured materials, enabling us to readily include the effect of material excitations for aloof electron trajectories. In section 2, we review a quantization scheme of the electromagnetic field in the presence of macroscopic and lossy media, extending a previous Coulomb gauge formulation [12] to the temporal gauge, which we find more suitable to deal with the noted interaction. We continue by showing that vacuum fluctuations induce both phase shifts and decoherence in an Aharonov–Bohm-like configuration. In section 3, we derive a scalar quantum electrodynamics (QED) Hamiltonian that represents to a good approximation the evolution of an electron wave function at energy scales typical of electron microscope setups, and further provide an analytical demonstration that the vacuum phase shift can transversally modulate the electron beam. In section 5, we discuss the phase produced on electrons moving parallel to either perfect or real planar conductor surfaces, whereas in section 6 we analyze far-field diffraction induced by either a planar surface or a small particle. We anticipate that these theoretical results could be corroborated in either interference or angle-resolved experiments.

In brief, we discuss a general theory of the interaction between fast electrons and electromagnetic modes in the vicinity of material media, leading to the emergence of a quantum phase imprinted on the electron transverse wave function. For aloof interaction with a planar surface, this phase is related to the Aharonov–Bohm effect due to the image potential [7], a result that we extend to arbitrarily shaped structures, for which we find that the quantum phase under discussion coincides with the Aharonov–Bohm effect associated with half (i.e., the image) of the self-induced electron vector potential in a gauge with vanishing scalar potential. We illustrate the effect that such phase has on a free electron by investigating two different experimental scenarios: a holographic measurement in which one compares the phase of an electron wave function component passing near a sample with the phase of another component that does not interact with the sample; and a diffraction measurement in which the electron distribution in the far-field Fourier plane is modified by the dependence of the imprinted phase on transverse beam coordinates.

2. Vacuum phase shift in the presence of macroscopic media

2.1. Macroscopic QED in the temporal gauge

Macroscopic QED has been extensively developed in the Coulomb gauge [12]. However, we find it more convenient to work in the temporal gauge (i.e., a gauge in which the scalar potential vanishes) to describe the interaction between free electrons and the electromagnetic fields in the presence of material boundaries. The constitutive relations connecting the frequency components of the field and vector potential operators then reduce to (in Gaussian units)

$$\begin{aligned}\hat{\mathbf{E}}(\mathbf{r}, \omega) &= \frac{i\omega}{c} \hat{\mathbf{A}}(\mathbf{r}, \omega), \\ \hat{\mathbf{B}}(\mathbf{r}, \omega) &= \nabla \times \hat{\mathbf{A}}(\mathbf{r}, \omega),\end{aligned}$$

where the vector potential operator $\hat{\mathbf{A}}$ is taken to satisfy the wave equation

$$\nabla \times \nabla \times \hat{\mathbf{A}}(\mathbf{r}, \omega) - \frac{\omega^2}{c^2} \epsilon(\mathbf{r}, \omega) \hat{\mathbf{A}}(\mathbf{r}, \omega) = \frac{4\pi}{c} \hat{\mathbf{j}}^{\text{noise}}(\mathbf{r}, \omega). \quad (1)$$

Here, we assume a linear local nonmagnetic response that is fully captured by the complex frequency-dependent permittivity $\epsilon(\mathbf{r}, \omega)$, which is required to satisfy causality and the Kramers–Kronig relations. We introduce a noise current $\hat{\mathbf{j}}^{\text{noise}}$ to describe the dissipation produced by coupling between the electromagnetic field and matter. More precisely, we construct this current as [12]

$$\hat{\mathbf{j}}^{\text{noise}}(\mathbf{r}, \omega) = \omega \sqrt{\hbar \text{Im}\{\epsilon(\mathbf{r}, \omega)\}} \mathbf{f}(\mathbf{r}, \omega), \quad (2)$$

where we define bosonic operators $\mathbf{f}(\mathbf{r}, \omega)$ and $\mathbf{f}^\dagger(\mathbf{r}, \omega)$ that follow the commutation relations

$$[\hat{f}_i(\mathbf{r}, \omega), \hat{f}_{i'}^\dagger(\mathbf{r}', \omega')] = 0, \quad (3)$$

$$[\hat{f}_i(\mathbf{r}, \omega), \hat{f}_{i'}^\dagger(\mathbf{r}', \omega')] = \delta_{ii'} \delta(\mathbf{r} - \mathbf{r}') \delta(\omega - \omega'), \quad (4)$$

and whose evolution is ruled by the radiation Hamiltonian [12]

$$\hat{\mathcal{H}}_{\text{rad}} = \int d^3\mathbf{r} \int_0^\infty d\omega \hbar\omega \mathbf{f}^\dagger(\mathbf{r}, \omega) \cdot \mathbf{f}(\mathbf{r}, \omega).$$

Additionally, by combining equations (2)–(4), these operators are found to satisfy the commutation relations

$$[\hat{j}_i^{\text{noise}}(\mathbf{r}, \omega), \hat{j}_j^{\text{noise}}(\mathbf{r}', \omega')] = 0, \quad (5)$$

$$[\hat{j}_i^{\text{noise}}(\mathbf{r}, \omega), (\hat{j}_{i'}^{\text{noise}}(\mathbf{r}', \omega'))^\dagger] = \hbar\omega^2 \text{Im}\{\epsilon(\mathbf{r}, \omega)\} \delta_{i,i'} \delta(\mathbf{r} - \mathbf{r}') \delta(\omega - \omega'). \quad (6)$$

A formal solution of equation (1) is given by

$$\hat{\mathbf{A}}(\mathbf{r}, \omega) = -4\pi c \int d^3\mathbf{r}' G(\mathbf{r}, \mathbf{r}', \omega) \hat{j}^{\text{noise}}(\mathbf{r}', \omega), \quad (7)$$

where $G(\mathbf{r}, \mathbf{r}', \omega)$ is the electromagnetic Green tensor satisfying the relation

$$\nabla \times \nabla \times G(\mathbf{r}, \mathbf{r}', \omega) - \frac{\omega^2}{c^2} \epsilon(\mathbf{r}, \omega) G(\mathbf{r}, \mathbf{r}', \omega) = -\frac{1}{c^2} \delta(\mathbf{r} - \mathbf{r}'). \quad (8)$$

Finally, by combining equations (5)–(7), the commutation relations of the vector potential become

$$[\hat{A}_i(\mathbf{r}, \omega), \hat{A}_{i'}(\mathbf{r}', \omega')] = 0, \quad (9)$$

$$[\hat{A}_i(\mathbf{r}, \omega), \hat{A}_{i'}^\dagger(\mathbf{r}', \omega')] = 16\pi^2 c^2 \hbar \delta(\omega - \omega') \text{Im}\{-G_{i,i'}(\mathbf{r}, \mathbf{r}', \omega)\}, \quad (10)$$

where we have made use of the identity [12]

$$\sum_{i''} \int d^3\mathbf{r}'' \text{Im}\{\epsilon(\mathbf{r}'', \omega)\} G_{i,i''}(\mathbf{r}, \mathbf{r}'', \omega) G_{i'',i'}^*(\mathbf{r}', \mathbf{r}'', \omega) = -\frac{1}{\omega^2} \text{Im}\{G_{i,i'}(\mathbf{r}, \mathbf{r}', \omega)\}$$

in order to evaluate the commutator in equation (10).

From these relations, we can work out the time-dependent commutator $[\hat{A}_i(\mathbf{r}, t), \hat{A}_{i'}(\mathbf{r}', t')]$, where $\hat{\mathbf{A}}(\mathbf{r}, t) = e^{i\hat{\mathcal{H}}_{\text{rad}}t/\hbar} \hat{\mathbf{A}}(\mathbf{r}) e^{-i\hat{\mathcal{H}}_{\text{rad}}t/\hbar}$, by noting that the potential frequency components are related to the time-dependent components through the relation [13]

$$\hat{\mathbf{A}}(\mathbf{r}, t) = \int_0^\infty \frac{d\omega}{2\pi} e^{-i\omega t} \hat{\mathbf{A}}(\mathbf{r}, \omega) + \text{h.c.},$$

which together with equations (9) and (10) lead to

$$[\hat{A}_i(\mathbf{r}, t), \hat{A}_{i'}(\mathbf{r}', t')] = 8ic^2 \hbar \int_0^\infty d\omega \sin[\omega(t - t')] \text{Im}\{G_{i,i'}(\mathbf{r}, \mathbf{r}', \omega)\}. \quad (11)$$

As in vacuum, this commutator is a purely imaginary c-number, from which we can calculate the retarded electromagnetic Green tensor, defined as

$$G_{i,i'}^{\text{R}}(\mathbf{r}, \mathbf{r}', t - t') = \frac{-i}{4\pi\hbar c^2} [\hat{A}_i(\mathbf{r}, t), \hat{A}_{i'}(\mathbf{r}', t')] \theta(t - t'). \quad (12)$$

Incidentally, using the fact that $G(\mathbf{r}, \mathbf{r}', \omega)$ satisfies the Kramers–Kronig relations, as well as the causality property $G(-\omega) = G^*(\omega)$, we find

$$G_{i,i'}^{\text{R}}(\mathbf{r}, \mathbf{r}', \omega) = \int_{-\infty}^\infty dt e^{i\omega t} G_{i,i'}^{\text{R}}(\mathbf{r}, \mathbf{r}', t), \quad (13)$$

so the quantum retarded Green tensor coincides with the classical Green tensor defined by equation (8).

2.2. Vacuum phase shift

We now obtain an expression for the elastic electron amplitude under interaction with a macroscopic quantized electromagnetic field. We consider an Aharonov–Bohm-like experiment in which the electron wave function is split into two paths (1 and 2). Before interaction with the electromagnetic field, the system density matrix is

$$\rho(t_0) = [|\psi_1(t_0)\rangle\langle\psi_1(t_0)| + |\psi_2(t_0)\rangle\langle\psi_2(t_0)| + |\psi_2(t_0)\rangle\langle\psi_1(t_0)| + |\psi_1(t_0)\rangle\langle\psi_2(t_0)|] \otimes \sigma(t_0),$$

where $\sigma(t_0)$ stands for the initial state of the photon field at time t_0 , while $|\psi_1(t_0)\rangle$ and $|\psi_2(t_0)\rangle$ are the electron states in paths 1 and 2, respectively. We take the interaction between the electromagnetic field and the electron to be described by a minimal coupling Hamiltonian in the temporal gauge, which in the interaction picture reads

$$\hat{H}(t) = -\frac{1}{c} \int d^3\mathbf{r} \hat{\mathbf{A}}(\mathbf{r}, t) \cdot \mathbf{j}(\mathbf{r}, t).$$

Assuming the electron current to be well described by its classical version on each of the two electron paths, we can write the electron density matrix at a later time $t > t_0$ as

$$\begin{aligned} \rho_e(t) = & |\psi_1(t_0)\rangle\langle\psi_1(t_0)| + |\psi_2(t_0)\rangle\langle\psi_2(t_0)| + |\psi_2(t_0)\rangle\langle\psi_1(t_0)| \text{Tr}\{\hat{S}_2\sigma(t_0)\hat{S}_1^\dagger\} \\ & + |\psi_1(t_0)\rangle\langle\psi_2(t_0)| \text{Tr}\{\hat{S}_1\sigma(t_0)\hat{S}_2^\dagger\}, \end{aligned} \quad (14)$$

where $\hat{S}_j = T e^{(-i/\hbar)\int_{t_0}^t dt' \hat{H}_j(t')}$ is the time-ordered evolution operator for the current along path $j = 1$ or 2, and we have traced out the photon degrees of freedom. The first two terms on the right-hand side of equation (14) represent the part of the electron wave function that is not affected by interaction with the electromagnetic field. The remaining two terms describe the coherence of the electron state. We now take the initial photon density matrix to be in a thermal state at temperature T and use the fact that the commutator between the vector potentials is a pure imaginary c -number (equation (11)) in order to rigorously disregard time ordering by using Wick's theorem [14]. By doing so, we obtain

$$\hat{S}_j = e^{i\chi_j} e^{-\frac{i}{\hbar}\int_{t_0}^t dt' \hat{H}_j(t')} = e^{i\chi_j} \hat{U}_j,$$

which, by going from $t_0 = -\infty$ to $t = \infty$, leads to

$$\langle \hat{S}_2^\dagger \hat{S}_1 \rangle_T = e^{i(\chi_1 - \chi_2)} \langle \hat{U}_2^\dagger \hat{U}_1 \rangle_T$$

with phase shifts given by

$$\chi_j = \frac{i}{2\hbar^2 c^2} \int_{-\infty}^{\infty} dt \int_{-\infty}^{\infty} dt' \int d^3\mathbf{r} \int d^3\mathbf{r}' \mathbf{j}_j(\mathbf{r}, t) \cdot [\hat{\mathbf{A}}(\mathbf{r}, t), \hat{\mathbf{A}}(\mathbf{r}', t')] \cdot \mathbf{j}_j(\mathbf{r}', t'). \quad (15)$$

Now, we use the Baker–Campbell–Hausdorff formula to recombine the evolution of the two paths, leading to

$$\langle \hat{S}_2^\dagger \hat{S}_1 \rangle_T = e^{i(\chi_1 - \chi_2)} e^{i\varphi} e^P,$$

where we have

$$\varphi = \frac{-i}{2\hbar^2 c^2} \int_{-\infty}^{\infty} dt' \int_{-\infty}^{\infty} dt \int d^3\mathbf{r} \int d^3\mathbf{r}' \mathbf{j}_2(\mathbf{r}', t') \cdot [\hat{\mathbf{A}}(\mathbf{r}', t'), \hat{\mathbf{A}}(\mathbf{r}, t)] \cdot \mathbf{j}_1(\mathbf{r}, t), \quad (16)$$

$$P = \frac{-1}{2\hbar^2 c^2} \int_{-\infty}^{\infty} dt \int_{-\infty}^{\infty} dt' \int d^3\mathbf{r} \int d^3\mathbf{r}' \mathbf{j}_{1,2}(\mathbf{r}, t) \cdot \langle \hat{\mathbf{A}}(\mathbf{r}, t) \hat{\mathbf{A}}(\mathbf{r}', t') \rangle_T \cdot \mathbf{j}_{1,2}(\mathbf{r}', t'), \quad (17)$$

and $\mathbf{j}_{1,2} = \mathbf{j}_1 - \mathbf{j}_2$. In this derivation, we have used the fact that $\hat{\mathbf{A}}(\mathbf{r}, t)$ is linear in the field operators, and therefore $\langle \hat{\mathbf{A}}(\mathbf{r}, t) \rangle_T = 0$ (see equations (2) and (7)), which leads to a cumulant expansion limited only to the second-order term [15]. The phase shift given by equation (16) relates to the interference between the two paths due to photon emission. This is clear by noticing that it appears only because of the cyclic property of the trace, which allows us to obtain the product $\hat{S}_2^\dagger \hat{S}_1$. In contrast, the expression in equation (17) is guaranteed to be a real number, so it represents the total decoherence experienced by the electron, which has been extensively studied from both theoretical [9, 16–18] and experimental [19–21] fronts. Importantly, it should be noted that, although the impressive increase of accuracy achieved in recent experiments served to rule out alternative theories, further decrease in experimental error is still needed to conclusively support a physical model [18]. The path-dependent phase and decoherence, which can affect

the fringes observed in an interference experiment, was derived as a dynamical scattering correction to the electron virtual interaction with sample excitations in a pioneering work [10] that related it to the so-called optical potential [11, 22, 23]. A subsequent formulation of such phase was then separately given in the context of quantum field theory [7] assuming zero temperature and neglecting inelastic losses, while an extension to finite temperature was later presented [15]. However, not much attention has so far been paid to the vacuum phase shift χ_j (equation (15)) and the role played by dissipation and finite conductivity in metallic structures, on which we focus here using a macroscopic QED formalism.

We find it useful to rewrite the phase shift of equation (15) in terms of the electromagnetic Green tensor by using equations (12) and (13). This allows us to write

$$\chi_j = \frac{2}{\hbar} \int_{-\infty}^{\infty} dt \int_{-\infty}^{\infty} dt' \int_0^{\infty} d\omega \int d^3\mathbf{r} \int d^3\mathbf{r}' \cos[\omega(t-t')] \times \mathbf{j}_j(\mathbf{r}, t) \cdot \text{Re}\{-G(\mathbf{r}, \mathbf{r}', \omega)\} \cdot \mathbf{j}_j(\mathbf{r}', t'), \quad (18)$$

where we have also used the Onsager reciprocity relation $G(\mathbf{r}, \mathbf{r}', \omega) = G^T(\mathbf{r}', \mathbf{r}, \omega)$. Now, if we consider the electron to be a point particle traveling along the z direction with constant velocity v and fixed transverse coordinates $\mathbf{R}_j = (x_j, y_j)$ (different for each of the two paths $j = 1$ and 2), the electron current is

$$\mathbf{j}_j(\mathbf{r}, t) = -ev \delta(z - vt) \delta(\mathbf{R} - \mathbf{R}_j) \hat{\mathbf{z}}, \quad (19)$$

which upon insertion into equation (18) leads to the expression

$$\chi_j = \frac{2e^2}{\hbar} \int_0^{\infty} d\omega \int_{-\infty}^{\infty} dz \int_{-\infty}^{\infty} dz' \cos\left[\frac{\omega}{v}(z-z')\right] \text{Re}\{-G_{z,z}(\mathbf{R}_j, z, \mathbf{R}_j, z', \omega)\} \quad (20)$$

for the impact-parameter-dependent electron phase shift. This result clearly emphasizes the fact that the quantum phase is the integral of a nonresonant quantity (the real part of the Green tensor), and thus it is expected to be small, although the numerical examples discussed below reveal a measurable effect. In more physical terms, the electron has to undergo an even number of virtual inelastic processes during its interaction with the sample before recovering its initial energy, so the phase change is at least a second-order process (indeed it arises from a commutator), although its effect is accumulated over an infinite number of electromagnetic modes that renders it non-negligible. We also remark that the phase does not depend on how the electromagnetic modes are populated, so it takes the same value if the sample starts from the ground state or from an excited state.

For completeness, we calculate the decoherence from equation (17), which requires the evaluation of the thermal average of the vector potentials,

$$\langle \hat{A}_i(\mathbf{r}, t) \hat{A}_{i'}(\mathbf{r}', t') \rangle_T = -4\hbar c^2 \int_0^{\infty} d\omega \text{Im}\{G_{i,i'}(\mathbf{r}, \mathbf{r}', \omega)\} \left[2n_T(\omega) \cos[\omega(t-t')] + e^{-i\omega(t-t')} \right].$$

Upon insertion of this expression into equation (17), using again the Onsager reciprocity relation and the Bose–Einstein distribution $n_T(\omega)$ at temperature T and frequency ω , we find

$$P = \frac{2}{\hbar} \int_0^{\infty} d\omega \int_{-\infty}^{\infty} dt \int_{-\infty}^{\infty} dt' \int d^3\mathbf{r} \int d^3\mathbf{r}' \cos[\omega(t-t')] [2n_T(\omega) + 1] \times \mathbf{j}_{1,2}(\mathbf{r}, t) \cdot \text{Im}\{G(\mathbf{r}, \mathbf{r}', \omega)\} \cdot \mathbf{j}_{1,2}(\mathbf{r}', t').$$

Considering now the two parallel paths described by the currents of equation (19), the decoherence takes the simple form

$$P = \frac{-1}{2} \int_0^{\infty} d\omega [2n_T(\omega) + 1] [\Gamma_{\text{EELS}}(\mathbf{R}_1, \mathbf{R}_1, \omega) + \Gamma_{\text{EELS}}(\mathbf{R}_2, \mathbf{R}_2, \omega) - \Gamma_{\text{EELS}}(\mathbf{R}_1, \mathbf{R}_2, \omega) - \Gamma_{\text{EELS}}(\mathbf{R}_2, \mathbf{R}_1, \omega)], \quad (21)$$

where

$$\Gamma_{\text{EELS}}(\mathbf{R}_j, \mathbf{R}_j, \omega) = \frac{4e^2}{\hbar} \int_{-\infty}^{\infty} dz \int_{-\infty}^{\infty} dz' \cos\left[\frac{\omega}{v}(z-z')\right] \text{Im}\{-G_{z,z}(\mathbf{R}_j, z, \mathbf{R}_j, z', \omega)\}$$

(compare this expression with equation (20)), so the first two terms inside the ω integral of equation (21) arise from the separate-path electron energy-loss spectroscopy probabilities (i.e., $\Gamma_{\text{EELS}}(\mathbf{R}_j, \mathbf{R}_j, \omega)$ is the EELS probability for an electron following path j [24]), whereas the last two terms stand for the inelastic path-interference contribution, all of which are weighted by a thermal factor that results from the sum of electron energy losses ($\propto n_T + 1$) and gains ($\propto n_T$).

2.3. Quantum phase in nonlocal media

We have so far considered materials characterized a frequency-dependent dielectric function $\epsilon(\mathbf{r}, \omega)$ that bears a local dependence on spatial position \mathbf{r} . While this assumption is generally safe to describe the response of dielectric optical cavities and plasmons in noble metal nanostructures with size features larger than ~ 10 nm, it becomes inaccurate in smaller particles [25, 26], in strongly nonlocal materials such as graphene [27], or in the analysis of free-electron interactions with tightly bound modes near metal surfaces [28], where quantum confinement, electron spill-out [29, 30], and the finite ~ 1 nm screening length [26, 31] contribute to make the material response nonlocal. A more complete description requires the use of a nonlocal dielectric function $\epsilon(\mathbf{r}, \mathbf{r}', \omega)$, where the displacement at \mathbf{r} depends on the electric field at different positions \mathbf{r}' . Unfortunately, a first-principles description of such function is only feasible for relatively simple geometries (e.g., planar surfaces and ultrathin films, as well as molecules and atomic clusters with up to a few hundred atoms). A classical hydrodynamic model of the conduction electron gas in metals [32–34] provides a simple description of nonlocal effects that has been extensively used to study inelastic electron interactions [35], while the specular reflection model [36] gives a general prescription to relate the nonlocal response of arbitrarily shaped nanostructures to the bulk nonlocal dielectric function [26]. In this context, the leading linear-order nonlocal correction in the surface response function captured by the Feibelman d parameters [37] has recently been revisited as a powerful tool to incorporate nonlocal effects in the electromagnetic response of metallic nanostructures [38]. Here, we do not enter into the details of the calculation of $\epsilon(\mathbf{r}, \mathbf{r}', \omega)$ and simply argue that the local description of the preceding sections remains essentially unchanged when nonlocal effects are taken into consideration. Indeed, equation (7) represents again the complete solution of Maxwell's equations with the Green tensor satisfying a generalization of equation (8):

$$\nabla \times \nabla \times G(\mathbf{r}, \mathbf{r}', \omega) - \frac{\omega^2}{c^2} \int d^3 \mathbf{r}'' \epsilon(\mathbf{r}, \mathbf{r}'', \omega) G(\mathbf{r}'', \mathbf{r}', \omega) = -\frac{1}{c^2} \delta(\mathbf{r} - \mathbf{r}').$$

Following reference [39], we impose the commutation relations

$$[\hat{j}_i^{\text{noise}}(\mathbf{r}, \omega), (\hat{j}_i^{\text{noise}}(\mathbf{r}', \omega'))^\dagger] = \hbar \omega^2 \text{Im}\{\epsilon(\mathbf{r}, \mathbf{r}', \omega')\} \delta_{i,i'} \delta(\omega - \omega')$$

for the noise currents and exploit the identity

$$\begin{aligned} & \sum_{i''} \int d^3 \mathbf{r}'' \int d^3 \mathbf{r}''' \text{Im}\{\epsilon(\mathbf{r}'', \mathbf{r}''', \omega)\} G_{i,i''}(\mathbf{r}, \mathbf{r}'', \omega) G_{i'',i'''}^*(\mathbf{r}', \mathbf{r}''', \omega) \\ & = -\frac{1}{\omega^2} \text{Im}\{G_{i,i'}(\mathbf{r}, \mathbf{r}', \omega)\}, \end{aligned}$$

to verify that equations (11) and (13) also hold for nonlocal media. Finally, because equation (15) does not depend on the explicit form of the electromagnetic potentials, as long as they are linear in the bosonic ladder operators, equations (20) and (21) retain its validity when including nonlocal effects in the definition of the Green tensor.

For translationally invariant samples, the dielectric response is only a function of position difference $\mathbf{r} - \mathbf{r}'$, which yields a local dielectric function in momentum space $\epsilon(\mathbf{q}, \omega)$. In particular, the response of noble metals deviates from the local limit mainly for $\omega/v_F \lesssim q$ [26], where v_F is the Fermi velocity. This allows us to estimate the importance of nonlocal effects for an electron passing at a distance ≥ 10 nm from a gold surface, which should involve components $q \leq 0.1$ nm⁻¹, so we can neglect nonlocal effects for energy exchanges $\hbar\omega \gtrsim \hbar q v_F \sim 0.1$ eV. As we show in section 5 below, the frequencies involved in the calculation of the phase for the examples considered in this work lie above this value, and therefore we can safely neglect nonlocal effects.

3. Quantum phase and Aharonov–Bohm effect in arbitrary geometries

As an extension of the explanation of the vacuum phase in terms of the Aharonov–Bohm effect associated with the image potential for an electron moving parallel to a perfect-conductor plate [7], we now argue that equation (20) results from the Aharonov–Bohm effect associated with a vector potential in the temporal gauge, but then this result is general for arbitrarily shaped structures. Indeed, direct application of the classical equivalent of equation (7) allows us to write the expectation value of the z component of the vector image potential produced by the electron current given by equation (19) as $A_z(\mathbf{r}, t) = (2ec) \int_0^\infty d\omega \int_{-\infty}^\infty dz' \text{Re}\{G_{z,z}(\mathbf{r}, \mathbf{R}_j, z', \omega) e^{i\omega(z'/v-t)}\}$, where an overall factor of 1/2 is introduced to reflect the fact that the potential arises from the electron self-interaction rather than from an external

source, and we use causality to reduce the ω integral to the positive frequency part. We now plug this expression into the phase $(-e/\hbar c)\int_{-\infty}^{\infty} dz A_z(\mathbf{R}_j, z, t)$ due to the Aharonov–Bohm effect [8], which is proportional to the integral of the vector potential acting on the electron along its trajectory $t = z/v$. Combining these expressions, we readily obtain equation (20), thus demonstrating that the quantum phase under discussion can be ascribed to the Aharonov–Bohm effect produced by the electron self-image potential for any sample geometry.

4. Direct derivation of the quantum phase from the explicit QED solution

4.1. QED effective Hamiltonian

The interaction of a beam electron with a quantized electromagnetic field in free space has been extensively studied in the framework of QED [14], while an extension of this theory to electromagnetic modes supported by macroscopic structures has been developed in the context of quantum optics and Casimir–Polder forces [40]. In this section, we follow the formalism of reference [41] to revisit the interaction with a classical field in a fully relativistic approach [42], assuming that the electromagnetic field can be expanded as a linear combination of either normal [43] or quasinormal [44] modes of negligible broadening. This allows us to write the vector potential in the temporal gauge as

$$\hat{\mathbf{A}} = \sum_j (-ic/\omega_j) \left[\vec{\mathcal{E}}_j(\mathbf{r})\hat{a}_j - \vec{\mathcal{E}}_j^*(\mathbf{r})\hat{a}_j^\dagger \right], \quad (22)$$

where the sum runs over electromagnetic boson modes j with creation and annihilation operators \hat{a}_j^\dagger and \hat{a}_j , frequency ω_j , and associated electric field $\vec{\mathcal{E}}_j(\mathbf{r})$.

We treat the electron using the Dirac equation in the minimal coupling scheme as [45, 46]

$$\left[m_e c^2 \beta + c \vec{\alpha} \cdot \left(\mathbf{p} + \frac{e}{c} \mathbf{A} \right) \right] \Psi = i\hbar \frac{\partial \Psi}{\partial t}, \quad (23)$$

where $\mathbf{p} = -i\hbar\nabla$ is the momentum operator, and β and $\vec{\alpha}$ are Dirac matrices. In what follows, we neglect negative-energy solutions (positrons) and expand the 4-component spinor as $\Psi = V^{-1/2} \sum_{\mathbf{k}} \psi_{\mathbf{k}} e^{i\mathbf{k}\cdot\mathbf{r} - iE_{\mathbf{k}}t/\hbar} \Psi_{\mathbf{k}}$, where [46]

$$\Psi_{\mathbf{k}} = A_{\mathbf{k}} \begin{bmatrix} \hat{\mathbf{s}} \\ B_{\mathbf{k}} \vec{\sigma} \cdot \mathbf{k} \hat{\mathbf{s}} \end{bmatrix}$$

are spinors of 2D spin polarization $\hat{\mathbf{s}}$, $\vec{\sigma}$ are Pauli matrices, and we define $A_{\mathbf{k}} = \sqrt{(E_{\mathbf{k}} + m_e c^2)/2E_{\mathbf{k}}}$ and $B_{\mathbf{k}} = \hbar c/(E_{\mathbf{k}} + m_e c^2)$. These spinors are eigenstates of the free-space Dirac equation $(m_e c^2 \beta + \hbar c \vec{\alpha} \cdot \mathbf{k}) \Psi_{\mathbf{k}} = E_{\mathbf{k}} \Psi_{\mathbf{k}}$ with energy $E_{\mathbf{k}} = c\sqrt{m_e^2 c^2 + \hbar^2 k^2}$. Assuming that the incident beam is well prepared with momentum components narrowly peaked around a central value \mathbf{k}_0 and that the interaction with the electromagnetic field does not produce large departures from this central value (i.e., $|\mathbf{k} - \mathbf{k}_0| \ll k_0$), we can linearize the free-electron energy in the sum over momenta as $E_{\mathbf{k}} \approx E_0 + (\hbar^2 c^2/E_0) \mathbf{k}_0 \cdot (\mathbf{k} - \mathbf{k}_0)$, which leads to an approximate version of the free-electron Hamiltonian $\hat{\mathcal{H}}_0 \approx E_0 - (\hbar^2 c^2/E_0) \mathbf{k}_0 \cdot (i\nabla + \mathbf{k}_0)$. Here, $E_0 = E_{k_0}$ and we have replaced \mathbf{k} by $-i\nabla$. We now insert this expression into equation (23) and approximate $\Psi_{\mathbf{k}}$ by $\Psi_{\mathbf{k}_0}$. Putting these elements together, we can finally rewrite equation (23) as

$$\left[E_0 - \hbar \mathbf{v} \cdot (i\nabla + \mathbf{k}_0) + (e\mathbf{v}/c) \cdot \mathbf{A} \right] \psi(\mathbf{r}, t) = i\hbar \frac{\partial \psi(\mathbf{r}, t)}{\partial t}, \quad (24)$$

where $\mathbf{v} = \hbar c^2 \mathbf{k}_0/E_0$ is the electron velocity, $E_0 = m_e c^2 \gamma$ and $\hbar \mathbf{k}_0 = m_e \mathbf{v} \gamma$ are the relativistic energy and momentum involving the Lorentz factor $\gamma = 1/\sqrt{1 - v^2/c^2}$, and the electron is now simply described by the scalar wave function $\psi(\mathbf{r}, t) = V^{-1/2} \sum_{\mathbf{k}} \psi_{\mathbf{k}} e^{i\mathbf{k}\cdot\mathbf{r} - iE_{\mathbf{k}}t/\hbar}$. We note that the above approximations are essentially ignoring spin effects and ponderomotive forces, which, for typical kinematical parameters of TEM electrons and for the light intensities and frequencies commonly employed in ultrafast nanophotonics and TEM experiments, can indeed be safely neglected.

We now describe the quantum radiation field by incorporating the radiation Hamiltonian $\hat{\mathcal{H}}_{\text{rad}}$ into equation (24) and using the quantum vector field $\hat{\mathbf{A}}$ instead of \mathbf{A} . In this effective theory, we now expand the wave function of the joint electron–field system as $\langle \mathbf{r} | \psi(t) \rangle = \sum_{\{n\}} \psi_{\{n\}}(\mathbf{r}, t) | \{n\} \rangle$ to describe a distinct scalar electron wave function $\psi_{\{n\}}(\mathbf{r}, t)$ for each of the possible number states $|\{n\}\rangle$ of the photonic boson ensemble, so that we finally write the Schrödinger equation

$$\hat{\mathcal{H}} \langle \mathbf{r} | \psi(t) \rangle = (\hat{\mathcal{H}}_0 + \hat{\mathcal{H}}_1) \langle \mathbf{r} | \psi(t) \rangle = i\hbar \frac{\partial \langle \mathbf{r} | \psi(t) \rangle}{\partial t} \quad (25)$$

with

$$\begin{aligned}\hat{\mathcal{H}}_0 &= \sum_j \hbar\omega_j \hat{a}_j^\dagger \hat{a}_j + E_0 - \hbar\mathbf{v} \cdot (i\nabla + \mathbf{k}_0), \\ \hat{\mathcal{H}}_1 &= (e\mathbf{v}/c) \cdot \hat{\mathbf{A}}.\end{aligned}$$

Taking the electron beam to be oriented along the z direction, we can write the ansatz solution

$$\langle \mathbf{r} | \psi(t) \rangle = \psi_0(\mathbf{r}, t) \sum_{\{n\}, \{\ell\}} \exp \left\{ i \sum_j \omega_j [\ell_j(z/v - t) - n_j t] \right\} f_{\{\ell\}}^{\{n\}}(\mathbf{r}) | \{n\} \rangle, \quad (26)$$

where $\psi_0(\mathbf{r}, t) = e^{i\mathbf{k}_0 \cdot \mathbf{r} - iE_0 t/\hbar} \phi(\mathbf{r} - \mathbf{v}t)$ is the electron wave function before interaction, while $\{\ell\}$ denotes the set of net numbers of photons exchanged with each of the modes $\ell_1, \dots, \ell_j, \dots$ (positive ℓ_j for photon absorption and negative for emission). By plugging equation (26) in equation (25), we find that the expansion coefficients in this expression must satisfy the differential equation [41]

$$\frac{df_{\{\ell\}}^{\{n\}}}{dz} = \sum_j \left[\sqrt{n_j} u_j^* f_{\ell_1, \dots, \ell_j+1, \dots}^{n_1, \dots, n_j-1, \dots} - \sqrt{n_j+1} u_j f_{\ell_1, \dots, \ell_j-1, \dots}^{n_1, \dots, n_j+1, \dots} \right], \quad (27)$$

where $u_j(z) = (e/\hbar\omega_j) \mathcal{E}_{j,z}(z) e^{-i\omega_j z/v}$. We note that equation (27) guarantees that $n_j + \ell_j$ is conserved along the interaction for each j , indicating that the number of excitations in the electron–boson system is preserved. This interesting property implies that equation (27) corresponds to the time evolution of a set of classically driven quantum harmonic oscillators, and therefore, it can be solved analytically [47]. Indeed, we can write the Hamiltonian of such harmonic oscillators as

$$\hat{\mathcal{H}} = \sum_j \left[\hbar\omega_j a_j^\dagger a_j + g_j(t) a_j + g_j^*(t) a_j^\dagger \right],$$

which, by introducing a general state $|\psi(t)\rangle = \sum_{\{n\}} \alpha_{\{n\}}(t) e^{-i\sum_j n_j \omega_j t} | \{n\} \rangle$ in the associated Schrödinger equation, leads to

$$i\hbar \frac{d\alpha_{\{n\}}}{dt} = \sum_j \left[\sqrt{n_j} g_j^* \alpha_{n_1, \dots, n_j-1, \dots} e^{i\omega_j t} + e^{-i\omega_j t} \sqrt{n_j+1} g_j \alpha_{n_1, \dots, n_j+1, \dots} \right]. \quad (28)$$

We immediately notice that equation (28) is equivalent to equation (27) if we make the substitutions

$$g_j e^{-i\omega_j t} \rightarrow -i\hbar v u_j, \quad t \rightarrow z/v. \quad (29)$$

This allows us to use the well-known solution of equation (28) in terms of the evolution operator [41, 48]

$$\hat{\mathcal{S}}(t, t_0) = e^{i\chi} \prod_j e^{\beta_j^* a_j^\dagger - \beta_j a_j}, \quad (30)$$

where $\beta_j(t, t_0) = \frac{i}{\hbar} \int_{t_0}^t dt' g_j(t') e^{-i\omega_j t'}$ and $\chi = -\frac{1}{\hbar} \sum_j \int_{t_0}^t dt' \text{Re}\{\beta_j(t', t_0) g_j^*(t') e^{i\omega_j t'}\}$. Incidentally, χ has been shown to be a Berry phase [49] in the context of a driven quantum harmonic oscillator, so it underlies the fact that the system under study is open, and not all the degrees of freedom are taken into account. We show below that the role of χ in the interaction with the electron is to produce a phase shift in its wave function. From equation (30), we can calculate the transition amplitudes between photon number states as

$$\langle \{n\} | \hat{\mathcal{S}}(t, t_0) | \{n_0\} \rangle = e^{i\chi} \prod_j A_j,$$

where we define the single-mode transition amplitude as [41]

$$\begin{aligned}A_j &= \langle n_j | e^{\beta_j^* a_j^\dagger - \beta_j a_j} | n_{0,j} \rangle = \sqrt{n_{0,j}! n_j!} e^{-|\beta_j|^2/2} (-\beta_j)^{n_{0,j}-n_j} \\ &\quad \times \sum_{n'_j=\max\{0, n_j-n_{0,j}\}}^{n_j} \frac{(-|\beta_j|^2)^{n'_j}}{n'_j! (n_{0,j} - n_j + n'_j)! (n_j - n'_j)!}.\end{aligned}$$

Now, we can perform the substitution (29) to solve our QED model by finding the coefficients of equation (26). In particular, taking the photon field state to be represented by some coefficients $\alpha_{\{n_0\}}$ right before interaction with the electron, we have

$$f_{\{\ell\}}^{\{n\}}(\mathbf{r}) = e^{i\chi(\mathbf{r})} \alpha_{\{n+\ell\}} \prod_j \sqrt{(n_j + \ell_j)! n_j!} e^{-|\beta_j(\mathbf{r})|^2/2} \\ \times (-\beta_j(\mathbf{r}))^{\ell_j} \sum_{n'_j=\max\{0, -\ell_j\}}^{n_j} \frac{(-|\beta_j(\mathbf{r})|^2)^{n'_j}}{n'_j! (\ell_j + n'_j)! (n_j - n'_j)!}, \quad (31)$$

where we have used the conservation of quantum numbers $n_{0,j} = \ell_j + n_j$ together with the fact that the initial electron state has $\ell_{0,j} = 0$ for all modes.

4.2. Elastic phase shift

Equation (31) represents the nonperturbative solution of the scattering between a scalar relativistic electron and all optical modes of the vacuum-sample system. There is obviously a part of the joint photon-electron state that represents the contribution without net photon (emission or absorption) exchanges. From the electron point of view, this component relates to elastic transitions and can be calculated from the associated density matrix after tracing out the photon degrees of freedom and isolating the zero quanta exchange term. Additionally, we are interested in samples held at some temperature, so we need to deal with thermal electromagnetic mixtures of states, which can be treated by calculating equation (31) for Fock states (i.e., taking $\alpha_{\{n\}} = \prod_j \delta_{n_j, n_{0,j}}$ for a given realization of Fock states $\{n_{0,j}\}$ before interaction with the electron) and averaging over thermal populations (i.e., over a Bose–Einstein distribution $p_{n_{0,j}} = e^{-(n_{0,j}+1)\hbar\omega_j/k_B T} / \bar{n}_j$ with average mode population $\bar{n}_j = 1 / [\exp(\hbar\omega_j/k_B T) - 1]$). We find an elastic electron density matrix

$$\rho_{\text{elastic}}(\mathbf{r}, \mathbf{r}') = \sum_{\{n_0\}} p_{\{n_0\}} \text{Tr} \{ \langle \mathbf{r} | \psi(t) \rangle \langle \mathbf{r}' | \psi(t) \rangle^\dagger \}_{\text{elastic}} \\ = \psi_0(\mathbf{r}, t) \psi_0^*(\mathbf{r}', t) \sum_{\{n_0\}} p_{\{n_0\}} f_{\{0\}}^{\{n_0\}}(\mathbf{r}) [f_{\{0\}}^{\{n_0\}}(\mathbf{r}')]^* \\ = \psi_0(\mathbf{r}, t) \psi_0^*(\mathbf{r}', t) e^{i[\chi(\mathbf{r}) - \chi(\mathbf{r}')] } D_{\text{elastic}}(\mathbf{r}, \mathbf{r}'), \quad (32)$$

where

$$D_{\text{elastic}}(\mathbf{r}, \mathbf{r}') = \prod_j e^{-[|\beta_j(\mathbf{r})|^2 + \beta_j(\mathbf{r}')|^2]/2} \\ \times \sum_{n_{0,j}} p_{n_{0,j}} (n_{0,j}!)^2 \sum_{n_j=0}^{n_{0,j}} \frac{(-|\beta_j(\mathbf{r})|^2)^{n_j}}{(n_j!)^2 (n_{0,j} - n_j)!} \sum_{n'_j=0}^{n_{0,j}} \frac{(-|\beta_j(\mathbf{r}')|^2)^{n'_j}}{(n'_j!)^2 (n_{0,j} - n'_j)!} \quad (33)$$

contains the remaining factors beyond $\exp[i\chi(\mathbf{r})]$ from equation (31). We note again that we are forcing the electromagnetic field to return to its initial state (i.e., we neglect emission and absorption of degenerate photonic states that leave the electron energy unaffected, although electron-mediated transfer of excitations between degenerate electromagnetic states could play a role in the elastically scattered electron signal). Interestingly, equation (32) includes both a phase shift $\chi(\mathbf{r})$ and a real decoherence amplitude $D_{\text{elastic}}(\mathbf{r}, \mathbf{r}')$ (see equation (31)), which we present in a self-contained form that can be computed for any general pure quantum state, in contrast to the specific case of a thermal mixture considered in equation (17). At $T = 0$, the second line of equation (33) reduces to 1, so $D_{\text{elastic}}(\mathbf{r}, \mathbf{r}') = e^{P(\mathbf{r}) + P(\mathbf{r}')}$, which allows us to define a position-dependent decoherence

$$P = \frac{-1}{2} \sum_j |\beta_j(\mathbf{r})|^2 \quad (34)$$

directly in the elastic electron wave function. Here, we focus on the elastic phase shift, which is given by [41]

$$\chi(\mathbf{r}) = - \sum_j \frac{e^2}{\hbar^2 \omega_j^2} \int_{-\infty}^z dz' \int_{-\infty}^{z'} dz'' \text{Im} \left\{ \mathcal{E}_{j,z}^*(\mathbf{R}, z'') \mathcal{E}_{j,z}(\mathbf{R}, z') \exp \left[-i \frac{\omega_j}{v} (z' - z'') \right] \right\}. \quad (35)$$

This phase shift can be shown to be equivalent to equation (15) by directly substituting the expansion of the vector potential (equation (22)) in the commutator, keeping in mind that the ladder operators of the electromagnetic modes evolve in time according to the free Hamiltonian $\hat{\mathcal{H}}_0$ as

$$a_j(t) = a_j e^{-i\omega_j t}, \quad a_j^\dagger(t) = a_j^\dagger e^{i\omega_j t},$$

and considering a classical current centered at $\mathbf{R} = \mathbf{R}_j$ as in equation (19). Finally, because the retarded Green tensor (equation (12)) satisfies equation (8) (see, for example, reference [50]), we conclude that equations (35) and (20) represent the same quantity.

5. Elastic diffraction by metallic plates

We now illustrate the vacuum-induced phase by considering electrons moving parallel to a planar conductor surface at a distance x from it (see inset in figure 1(a)). We take the conductor to span a large distance along the direction of motion compared with both x and any of the photon wavelengths effectively contributing to the electron–surface interaction. The Green tensor can then be written as the sum of free-space and scattered components $G^0 + G^s$. The phase shift arising from the free-space Green tensor G^0 is formally infinite, but it does not depend on the transverse coordinate of the electron, therefore becoming unobservable [7]. The remaining scattered component admits an analytical expression in terms of the Fresnel reflection coefficients r_p and r_s for p and s polarization [13],

$$G_{z,z}^s(\mathbf{R}, z, \mathbf{R}, z', \omega) = \frac{i}{2c^2} \int \frac{d^2 \mathbf{k}_\parallel}{(2\pi)^2} \frac{1}{k_\parallel^2 k_x} \exp [ik_z(z - z') + 2ik_x x] \left(r_p \frac{k_z^2 k_x^2}{k^2} - r_s k_y^2 \right), \quad (36)$$

where $k = \omega/c$, the integral extends over wave vectors $\mathbf{k}_\parallel = (k_y, k_z)$ parallel to the surface, and $k_x = \sqrt{\omega^2/c^2 - k_\parallel^2} + i0^+$ with the square root taken to yield a positive real part.

5.1. Perfect conductor

For a perfect electric conductor, we have Fresnel coefficients $r_p = 1$ and $r_s = -1$, which permit obtaining a closed-form expression from equation (20). We first note that the in-plane translational invariance of the Green tensor component in equation (36) allows us to replace one of the spatial integrals by the effective electron path length D , which, neglecting inelastic deflections occurring during the interaction, may be approximated by the length of the plate (we refer to reference [53], where the deflection due Johnson noise is estimated to produce a correction of only a few hundred nanometers in the effective length for $D = 10 \mu\text{m}$; additionally, figure 1(c) shows that the fraction of inelastically scattered electrons is, for example, ~ 0.1 at 300 K for an electron passing with velocity $v = 0.1 c$ at a distance of 10 nm from a 10- μm -long gold plate). The remaining integral over the difference $z - z'$ yields δ functions, leading to

$$\chi(x) = \frac{\alpha\pi}{c} D \int_0^\infty d\omega \int \frac{d^2 \mathbf{k}_\parallel}{(2\pi)^2} \left[\delta \left(k_z - \frac{\omega}{v} \right) + \delta \left(k_z + \frac{\omega}{v} \right) \right] \times \frac{e^{-2x\kappa_x}}{k_\parallel^2 \kappa_x} \left(\frac{k_z^2 \kappa_x^2}{k^2} - k_y^2 \right),$$

where $\kappa_x = \sqrt{k_\parallel^2 - \omega^2/c^2}$ and $\alpha \approx 1/137$ is the fine structure constant. We now perform the frequency integral using the delta functions and write the remaining 2D integral in polar coordinates $(k_z, k_y) = k_\parallel (\cos \theta, \sin \theta)$. We obtain

$$\chi(x) = \frac{\alpha}{2\pi} \frac{D}{\beta_e \gamma^2} \int_0^\infty dk_\parallel \int_{-\pi/2}^{\pi/2} d\theta \frac{\exp \left(-2k_\parallel x \sqrt{1 - \beta_e^2 \cos^2 \theta} \right)}{\sqrt{1 - \beta_e^2 \cos^2 \theta}},$$

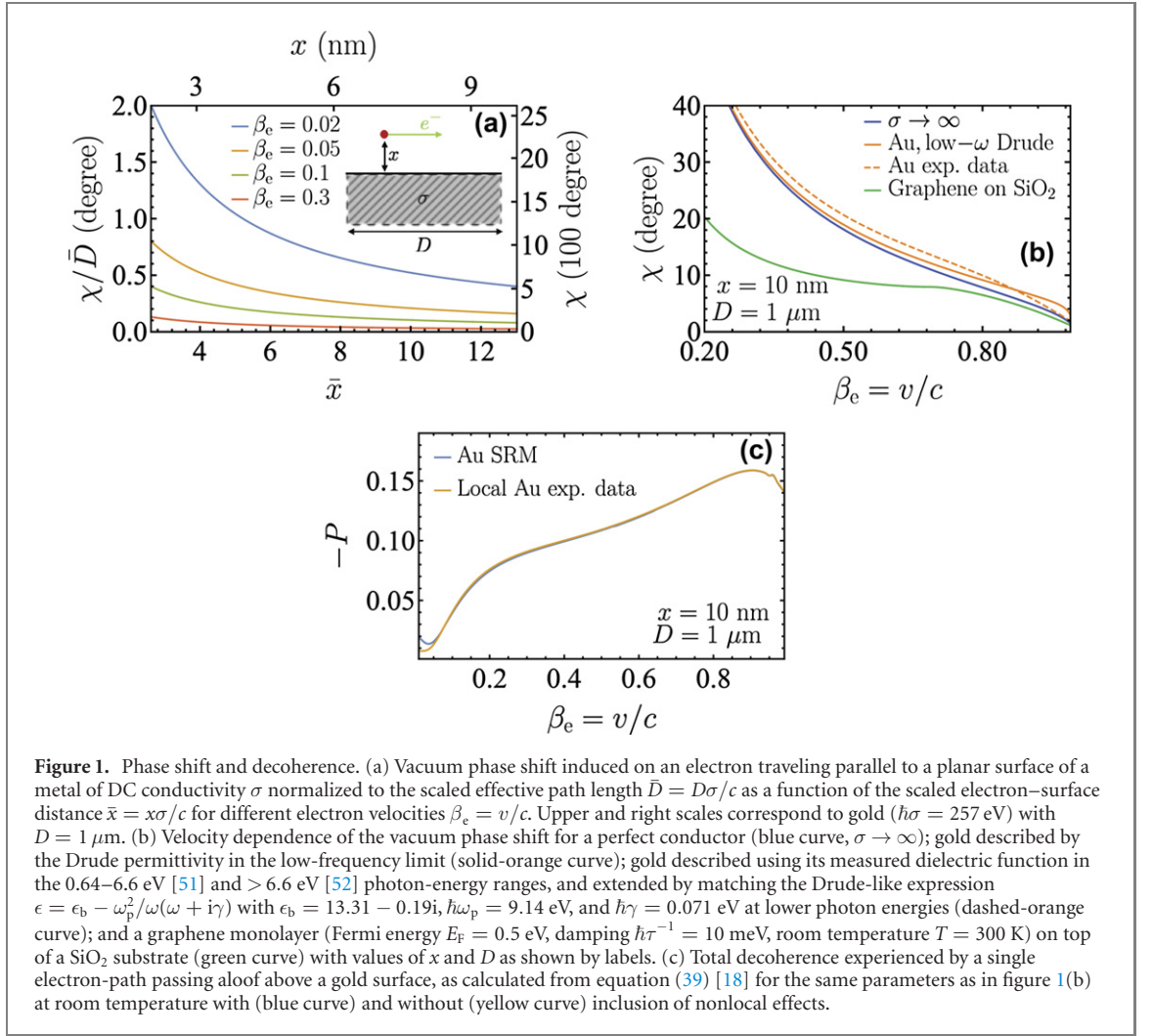
where $\beta_e = v/c$. Finally, using the integral $\int_{-\pi/2}^{\pi/2} dx (1 - a \cos^2 x)^{-1} = \pi/\sqrt{1-a}$ (equations (3.653-2) of reference [54]), we find

$$\chi(x) = \frac{\alpha D}{4x} \frac{1}{\beta_e \gamma}, \quad (37)$$

which coincides with the Aharonov–Bohm phase shift induced on a moving charge under the effect of its image potential, as pointed out in previous studies [7, 55].

5.2. Real conductor

We now extend the previous result to real metals by including inelastic losses in the material, which we model through a frequency-dependent local dielectric function $\epsilon(\omega)$. Inserting equation (36) into



equation (20) and following similar steps as in section 5.1, we find the phase

$$\chi = \frac{\alpha D}{2\pi\beta_e} \int_0^\infty dk_{\parallel} \int_{-\pi/2}^{\pi/2} d\theta \frac{\exp\left(-2xk_{\parallel}\sqrt{1-\beta_e^2\cos^2\theta}\right)}{\sqrt{1-\beta_e^2\cos^2\theta}} \times \text{Re}\{r_p - \beta_e^2(r_p\cos^2\theta - r_s\sin^2\theta)\}, \quad (38)$$

where the Fresnel coefficients $r_p = (\epsilon k_x - k'_x)/(\epsilon k_x + k'_x)$ and $r_s = (k_x - k'_x)/(k_x + k'_x)$, with $k_x = \sqrt{\omega^2/c^2 - k_{\parallel}^2}$ and $k'_x = \sqrt{\epsilon\omega^2/c^2 - k_{\parallel}^2}$, must be evaluated at frequency $\omega = vk_{\parallel}\cos\theta$. Equation (38) confirms the validity of neglecting nonlocal effects because for an electron with $\beta_e = 0.1$ passing 10 nm above the surface we have $\hbar\omega \approx \hbar v/x \sim 2$ eV (see discussion at the end of section 2.3); the local approximation starts failing at angles that make $\cos\theta$ small, and thus contribute only negligibly to the integral, and also at low velocities. Using the Drude approximation $\epsilon = 1 + 4\pi i\sigma/\omega$ for the metal dielectric function, where σ is the DC conductivity, we find from equation (38) the results presented in figure 1(a) for an electron moving above a gold surface ($\hbar\sigma \sim 257$ eV, upper and right axes) with different velocities $v = \beta_e c$. Finite conductivity in the real metal affects very little the decay of the phase shift as a function of electron velocity compared to equation (37), as shown in figure 1(b). We further corroborate good agreement with results obtained by using the measured dielectric function of gold taken from references [51, 52] (see figure 1(b)), which is in agreement with the intuition that low frequencies (i.e., those that are well captured by the Drude model) contribute dominantly for the surface-electron distances under consideration.

Upon inspection of equation (38), we find that the phase depends on metal conductivity σ and geometrical parameters (separation x and path length D) as $\chi = (D/x)F(\bar{x}, \beta_e)$, where F is a function of the scaled distance $\bar{x} = x\sigma/c$ and the electron velocity $v = \beta_e c$. This expression justifies the universal scaling used in figure 1(a) (left and lower axes). In particular, in the $\beta_e \ll 1$ limit, we can approximate

$r_p \approx 1 + i\omega/2\pi\sigma - \omega^2/4\pi^2\sigma^2$ and neglect β_e^2 terms inside the integral of equation (38) to obtain

$$\chi \approx \frac{\alpha D}{4x\beta_e} \left[1 - \left(\frac{\beta_e}{4\pi x} \right)^2 \right], \quad \beta_e \ll 1.$$

This expression shows that the perfect conductor approximation (equation (37)) describes well the phase shift in front of gold for slow electrons, in agreement with the results of figure 1(b).

The above results need to be contrasted with the effect of decoherence in order to determine whether the predicted phase shift may be observed in practice. As mentioned in section 2.2, decoherence was calculated in reference [18] by assuming local response and neglecting retardation effects. Here, we calculate decoherence from equation (21) including retardation and nonlocal effects in the EELS probability. For a single electron path running parallel to a planar surface, we have [24]

$$P = -\frac{De^2}{\pi\hbar v^2} \int_0^\infty d\omega \int_0^\infty \frac{dk_y}{k_{\parallel}^2} \operatorname{Re} \left\{ k_x e^{2ik_{xx}} \left[\left(\frac{k_y v}{k_x c} \right)^2 r_s - r_p \right] \right\}, \quad (39)$$

where $k_{\parallel} = \sqrt{\omega^2/v^2 + k_y^2}$. We introduce nonlocal effects in this expression by adopting the specular-reflection model [36] and using the Feibelman d -parameters approach [37]. Only the Fresnel coefficient

$$r_p = \frac{\epsilon k_x - k'_x + (\epsilon - 1)ik_{\parallel}^2 d_{\perp}}{\epsilon k_x + k'_x - (\epsilon - 1)ik_{\parallel}^2 d_{\perp}} \quad (40)$$

needs to be corrected [56], where [57]

$$d_{\perp} = -\frac{2}{\pi} \frac{\epsilon}{\epsilon - 1} \int_0^\infty \frac{dk}{k^2} \left[\frac{1}{\epsilon_{\text{NL}}(k, \omega)} - \frac{1}{\epsilon(\omega)} \right] \quad (41)$$

is the perpendicular Feibelman parameter and $\epsilon_{\text{NL}}(k, \omega)$ is the nonlocal metal permittivity. We approximate the latter following the prescription of reference [26]. Figure 1(c) confirms that nonlocal effects contribute only at low velocities for the electron–surface distances under consideration, and additionally, decoherence takes negligible values ~ 0.1 . We also find that low electron velocities are more favorable for the observation of interference fringes produced by the vacuum phase shift.

5.3. Graphene film

The above formalism allows us to discuss the quantum phase shift induced on a swift electron flying parallel to a graphene monolayer deposited on a semi-infinite substrate of permittivity ϵ . Describing graphene as a zero-thickness layer with local, frequency-dependent surface conductivity $\sigma_g(\omega)$, the phase of equation (20) can be easily computed from equation (38) by now writing the Fresnel coefficients as [58]

$$r_p = \frac{\epsilon k_x - k'_x + 4\pi\sigma_g k_x k'_x / \omega}{\epsilon k_x + k'_x + 4\pi\sigma_g k_x k'_x / \omega},$$

$$r_s = \frac{k_x - k'_x - 4\pi\sigma_g \omega / c^2}{k_x + k'_x + 4\pi\sigma_g \omega / c^2},$$

where k_x and k'_x are the out-of-plane light wave-vector components outside and inside the substrate (see expressions above), respectively. In order to numerically calculate the phase shift, we evaluate the graphene conductivity within the local-RPA model at finite temperature T using the analytical expression [59, 60]

$$\sigma_g(\omega) = \frac{e^2}{\pi\hbar^2} \frac{i}{\omega + i\tau^{-1}} \left\{ \mu^{\text{D}} - \int_0^\infty dE \frac{f_E - f_{-E}}{1 - 4E^2 / [\hbar^2(\omega + i\tau^{-1})^2]} \right\},$$

where $\mu^{\text{D}} = \mu + 2k_{\text{B}}T \log(1 + e^{-\mu/k_{\text{B}}T})$, τ is a phenomenological relaxation time, and $f_E = [e^{(E-\mu)/k_{\text{B}}T} + 1]^{-1}$ is the Fermi–Dirac distribution depending on graphene electron energy E and

chemical potential $\mu \approx \sqrt{\sqrt{(E_{\text{F}})^4 + (2 \log^2 4)(k_{\text{B}}T)^4} - (2 \log^2 4)(k_{\text{B}}T)^2}$ for a given Fermi energy E_{F} . In figure 1(b), we show the dependence of the resulting phase (equation (38)) on electron velocity for high-quality doped graphene ($E_{\text{F}} = 0.5$ eV, $\hbar\tau^{-1} = 10$ meV) supported on a silica substrate described by a permittivity ϵ taken from reference [52]. At high velocity, we recover the perfect-conductor limit because low frequencies are dominant in that regime.

6. Elastic diffraction by a small particle

We now consider a geometry lacking any translational symmetry by computing the vacuum phase for an electron interacting with a small particle, the electromagnetic response of which is described within the dipolar approximation in terms of the particle polarizability tensor α . The scattering part of the associated Green tensor admits an analytical expression in terms of the free-space Green tensor $G^0 = -(\omega^2/c^2 + \nabla \otimes \nabla) e^{i(\omega/c)|\mathbf{r}-\mathbf{r}'|} / (4\pi\omega^2|\mathbf{r}-\mathbf{r}'|)$ [24]:

$$G_{z,z}^s(\mathbf{R}, z, \mathbf{R}, z', \omega) = -4\pi\omega^2 \sum_{i,i'} G_{z,i}^0(\mathbf{R}, z, \mathbf{r}_0, \omega) \alpha_{i,i'} G_{i',z}^0(\mathbf{r}_0, \mathbf{R}, z', \omega), \quad (42)$$

where \mathbf{r}_0 is the particle position ($\mathbf{r}_0 = 0$ for simplicity) and the indexes i, i' run over Cartesian directions. In what follows, we consider a diagonal polarizability tensor α of components α_x, α_y , and α_z . Now, by plugging equation (42) into equation (20) and then using the integrals $\int_{-\infty}^{\infty} dz e^{i\omega z/v} e^{ikr}/r = 2K_0(\zeta)$ and $\int_{-\infty}^{\infty} dz e^{i\omega z/v} [e^{ikr}/r^2 + i e^{ikr}/kr^3] = 2icK_1(\zeta)/Rv\gamma$, where $r = \sqrt{R^2 + z^2}$ and $\zeta = \omega R/v\gamma$ (see equations (3.914-4) and (3.914-5) in reference [54], where we consider that $k = \omega/c + i0^+$ has a positive infinitesimal imaginary part), we obtain the expression

$$\chi(x, y) = \frac{2e^2}{\pi\hbar v^4 \gamma^2} \int_0^{\infty} \omega^2 d\omega \operatorname{Re} \left\{ \left[\frac{\alpha_x x^2 + \alpha_y y^2}{R^2} K_1^2 \left(\frac{\omega R}{v\gamma} \right) + \frac{\alpha_z}{\gamma^2} K_0^2 \left(\frac{\omega R}{v\gamma} \right) \right] \right\}.$$

For an isotropic particle ($\alpha = \alpha_x = \alpha_y = \alpha_z$), the phase depends only on radial distance R and this expression reduces to

$$\chi(R) = \frac{2e^2}{\pi\hbar v^4 \gamma^2} \int_0^{\infty} \omega^2 d\omega f \left(\frac{\omega R}{v\gamma} \right) \operatorname{Re} \{ \alpha \}, \quad (43)$$

where $f(\zeta) = K_1^2(\zeta) + K_0^2(\zeta)/\gamma^2$. We study below a small homogeneous sphere, for which the approximation $\alpha = 3c^3 t_1^E / 2\omega^3$ in terms of the dipolar electric Mie coefficient t_1^E captures retardation effects and compares well with full calculations of EELS [24]. This leads to a position-dependent decoherence (see equation (34) and the analytical result for the coupling coefficient β_j presented in reference [41])

$$P(R) = \frac{-2e^2}{\pi\hbar v^4 \gamma^2} \int_0^{\infty} \omega^2 d\omega f \left(\frac{\omega R}{v\gamma} \right) \operatorname{Im} \{ \alpha \} \quad (44)$$

at $T = 0$, which agrees with the expression obtained from the EELS probability for small spheres [24].

Incidentally, for a particle hosting a dominant sharp mode of frequency ω_0 , we can approximate $\alpha = A/(\omega_0 - \omega - i0^+)$, which upon insertion in equations (43) and (44) leads to

$$P(R) = \frac{-2e^2 A \omega_0^2}{\hbar v^4 \gamma^2} f \left(\frac{\omega_0 R}{v\gamma} \right), \quad (45)$$

$$\chi(R) = \frac{-2e^2 A \omega_0^2}{\hbar v^4 \gamma^2} g \left(\frac{\omega_0 R}{v\gamma} \right), \quad (46)$$

where

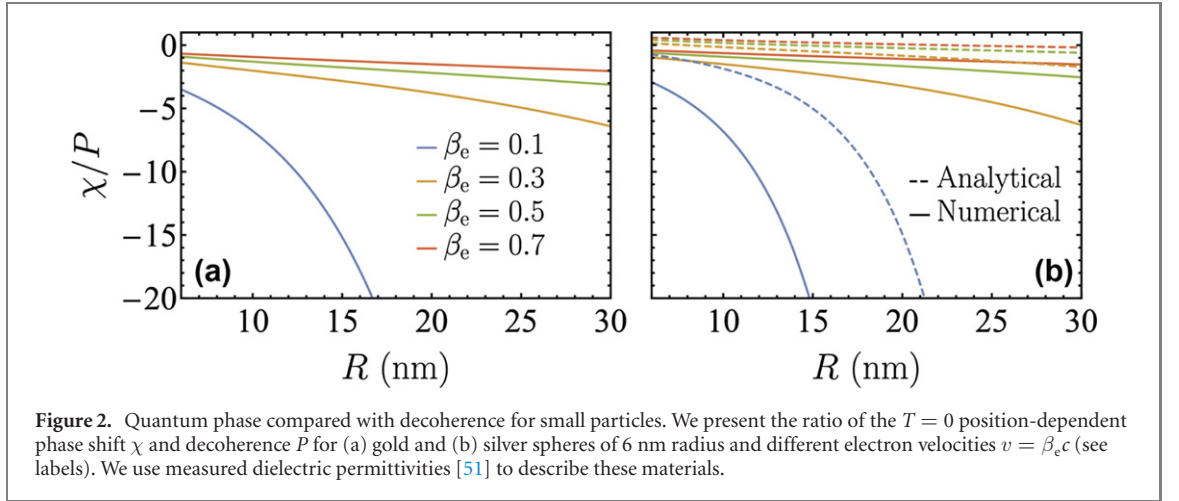
$$g(\theta) = \frac{1}{\pi} \operatorname{PV} \int_0^{\infty} \frac{x^2 dx}{x-1} f(x\theta),$$

and PV stands for the principal value. In electron microscopy one is interested in imaging without damaging, for which a high ratio $|\chi/P| = |g/f|$ becomes advantageous. We explore such ratio in figure 2 for the interaction with gold and silver spherical particles, where we find that χ can take much larger values than P (in particular, we find vacuum phase shifts $\chi \sim 3^\circ$ for the gold sphere at a distance $R = 15$ nm, see below), thus supporting the use of holography (i.e., measurement of the quantum phase) as an advantageous route to imaging without damaging compared with bright-field electron acquisition (i.e., resolving P). We present calculations based on direct use of equations (43) and (44) (solid curves in figure 2). For silver (figure 2(b)), which displays a well-defined plasmon mode, these results compare well with the analytical calculation obtained from equations (45) and (46) (broken curves).

7. Diffraction in the far-field

7.1. Interaction with a planar surface

Equation (20) shows a position-dependent phase shift that the electron wave function experiences after interaction with the electromagnetic vacuum. This phase shift may be observed through an interference experiment, as the one described in section 2, consisting in splitting an electron beam in two parts and



then recombining them after interaction of one of the components with the structure. The theory developed in section 4 shows how this phase affects the transverse component of the electron wave function, and consequently, an alternative to beam splitting techniques may be provided by a combined energy- and angle-resolved experiment. Indeed, the elastic component of the electron beam density matrix contains the vacuum phase through $\rho_{\text{elastic}}(\mathbf{r}, \mathbf{r}') = \psi_0(\mathbf{r}) \psi_0^*(\mathbf{r}') \exp\{i[\chi(\mathbf{r}) - \chi(\mathbf{r}')]\} D_{\text{elastic}}(\mathbf{r}, \mathbf{r}')$ (see equation (32)). We remark that, although we only study the effect of the quantum phase associated with vacuum fluctuations on elastic electron components, it also affects inelastic components, where a certain degree of coherence is preserved, which could be analyzed following the approach used to study inelastic electron holography [61]. Obviously, the elastic electron density $\rho_{\text{elastic}}(\mathbf{r}, \mathbf{r})$ is not modified, and therefore, it does not lead to any measurable effect if decoherence is neglected, as shown in figure 3(a), where only the x -dependent part of the wavefunction ψ_x is plotted.

In contrast, the diagonal coefficients of the electron density matrix in momentum space, which we calculate by Fourier-transforming the electron wave function as

$$\psi_{\text{elastic},\mathbf{Q}}(z) = \int d^2\mathbf{R} \psi_0(\mathbf{r}) \exp[i\chi(\mathbf{R}) + P(\mathbf{R}) - i\mathbf{Q} \cdot \mathbf{R}] \quad (47)$$

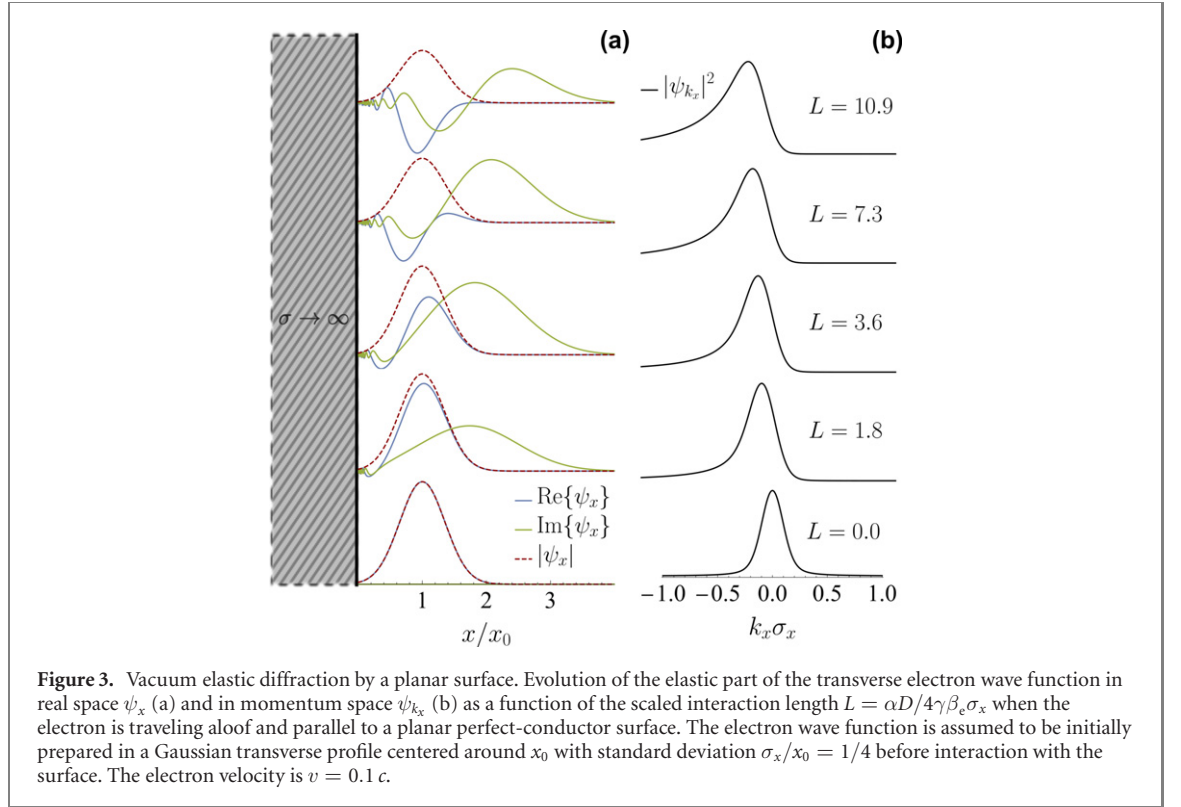
with $\mathbf{r} = (\mathbf{R}, z)$ and $\mathbf{R} = (x, y)$, display a dependence on the imprinted position-dependent quantum phase χ and decoherence P , with the latter expressed at $T = 0$ from equation (34). For illustration, we assume the initial electron wave function along the out-of-plane direction x to be well described by a Gaussian of standard deviation σ_x centered at a distance x_0 from the metallic plate. Since the electron wave function does not experience any change along in-plane directions, these Fourier components can be factorized. The only nontrivial component is thus $\psi_{k_x} \equiv \psi_{\text{elastic},k_x}$, the squared modulus of which presents an evolution as illustrated in figure 3(b) for an electron traveling parallel to a perfect conductor, which, as shown above, provides a good approximation to gold surfaces for the large values of x_0 under consideration, and furthermore results in $P = 0$. The presence of the distance-dependent phase shift given by equation (37) in the present case affects the out-of-plane electron wave function, which is progressively bent toward the surface, as expected from image charge attraction.

7.2. Interaction with a small object

Quantum-vacuum-induced diffraction can be equivalently quantified in terms of the electron current measured far from the scatterer. In particular, if we assume the interaction region to be limited to $z < z_1$, the acquired phase χ can be considered a function only of the transverse coordinates $\mathbf{R} = (x, y)$. Additionally, outside that region the elastic part of the scattered electron ψ_{elastic} must satisfy the Helmholtz equation $(\nabla^2 + k_0^2)\psi_{\text{elastic}} = 0$, where k_0 is the electron wave vector. We thus have for $z > z_1$

$$\psi_{\text{elastic}}(\mathbf{r}) = \int \frac{d^2\mathbf{Q}}{(2\pi)^2} \psi_{\text{elastic},\mathbf{Q}}(z_1) \exp[ik_{z,\mathbf{Q}}(z - z_1) + i\mathbf{Q} \cdot \mathbf{R}], \quad (48)$$

where $k_{z,\mathbf{Q}} = \sqrt{k_0^2 - Q^2 + i0^+}$ and $\psi_{\text{elastic},\mathbf{Q}}(z_1)$ is defined in equation (47). Equation (48) guarantees the continuity of the wave function at $z = z_1$. In the far-field limit ($k_0 r \gg 1$), equation (48) can be



approximated, using the stationary-phase method [62], as

$$\psi_{\text{elastic}}(\mathbf{r}) \approx -\frac{ik_0 \cos \theta}{2\pi} \psi_{\text{elastic}, \mathbf{Q}_f} \frac{e^{ik_0 r}}{r},$$

where $\mathbf{Q}_f = k_0 \mathbf{R}/r$ and $\cos \theta = z/r$. Taking now an incident beam with transverse Gaussian profile of width σ_R focused at $\mathbf{r} = (x_0, 0, 0)$ (i.e., an incident electron wave function $\psi_0(\mathbf{r}) \approx e^{ik_0 z - [(x-x_0)^2 + y^2]/4\sigma_R^2} / (2\pi\sigma_R^2 L)^{1/2}$ near the region of interaction with the particle, where L is the quantization length along the beam direction), we can calculate the electron current collected within a far-field solid angle $d\Omega$ as

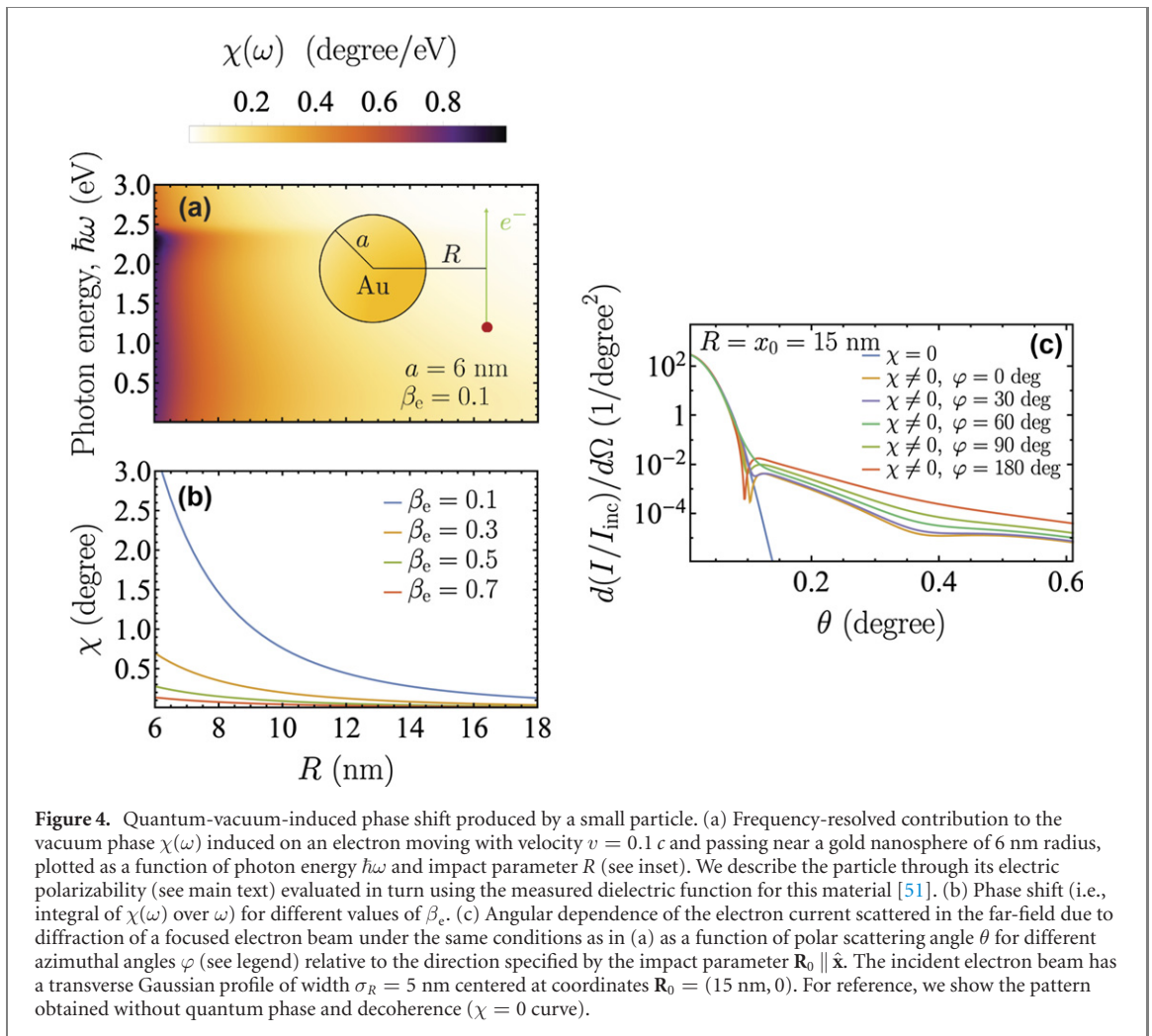
$$dI = (\hbar/m_e) \text{Im}\{\psi^* \hat{\mathbf{r}} \cdot \nabla \psi\} r^2 d\Omega = I_{\text{inc}} \frac{k_0^2 \cos^2 \theta}{4\pi^2} |\sqrt{L} \psi_{\text{elastic}, \mathbf{Q}_f}|^2 d\Omega, \quad (49)$$

where $I_{\text{inc}} = \hbar k_0/m_e L$. We use this expression to study the effect of vacuum fluctuations produced by interaction of the electron with a small particle, for which we apply the formalism of section 6, so we plug equation (43) into equations (47) to (49) and focus on a nanosphere of radius a located at the origin and described by its dipolar response. We obtain

$$\begin{aligned} \frac{dI}{d\Omega} &= I_{\text{inc}} \frac{k_0^2 \cos^2 \theta}{2\pi\sigma_R^2} e^{-x_0^2/2\sigma_R^2} \left| \int_0^\infty R dR \exp \left[-\frac{R^2}{4\sigma_R^2} + i\chi(R) + P(R) - \frac{\text{Re}\{\sqrt{a^2 - R^2}\}}{\lambda_e} \right] \right| \\ &\times I_0 \left[R \sqrt{\left(\frac{x_0}{2\sigma_R^2} - iQ_x \right)^2 - Q_y^2} \right]^2, \end{aligned} \quad (50)$$

where we use the notation $\mathbf{Q}_f = (Q_x, Q_y)$, the modified Bessel function I_0 is the result of applying the tabulated integral (3.937-2) in reference [54], and an elastic attenuation length λ_e is introduced to account for the depletion of the transmitted electron wave function due to heavy collisions inside the metal. We plot the resulting electron angular distribution calculated from equation (50) in figure 3(c) ($\chi \neq 0$ curves) for a gold nanosphere of radius $a = 6$ nm ($\ll \lambda_e$) and an electron beam of velocity $v = 0.1 c$, width $\sigma_R = 5$ nm, and impact parameter $x_0 = 15$ nm relative to the particle center. We further compare the scattering pattern with the one obtained in the absence of the nanoparticle (i.e., setting $\chi = 0$), which takes the analytical form (also assuming $a \ll \lambda_e$)

$$\frac{dI}{d\Omega} = I_{\text{inc}} \frac{2k_0^2 \sigma_R^2 \cos^2 \theta}{\pi} \exp(-2k_0^2 \sigma_R^2 \sin^2 \theta). \quad (51)$$



Reassuringly, for the large values of $k_0\sigma_R > 10^3$ under consideration, the right-hand side of equation (51) yields $I \approx I_{\text{inc}}$ when integrated over solid angle Ω . Remarkably, the influence of vacuum fluctuations modifies the electron wave function, introducing in the far-field current distribution an azimuthal dependence as well as substantial scattering up to $\theta \sim 1^\circ$, in contrast to the result obtained from the direct beam without particle-mediated coupling to vacuum fluctuations (see figure 4(c) and equation (51)).

8. Conclusion

In summary, we have shown that the elastic part of an electron beam has a phase shift imprinted in its transverse wave function dependence upon interaction with the vacuum electromagnetic field in the presence of a material structure. This effect, which can be attributed to fluctuations characterizing the quantum electromagnetic field, could be experimentally measured by means of either interference or diffraction of electron beams using an electron microscope. Specifically, our calculations predict that the aloof vacuum interaction of a $\beta_e = 0.1$ (~ 2.5 keV kinetic energy) electron with a planar gold surface results in a significant phase shift for a path length $D \sim 1 \mu\text{m}$ (see figure 1), which should produce discernible interference fringes only marginally affected by decoherence (see figure 1(c) and reference [18]). Indeed, the recombination of the two parts of the electron wave function $\psi_j e^{ix_j}$ following different paths $j = 1, 2$ that are affected by their corresponding phases χ_j leads to an electron probability at the detector $\propto |\psi_1|^2 + |\psi_2|^2 + 2 \text{Re}\{\psi_1\psi_2^* e^{i(\chi_1 - \chi_2)}\}$; when one of the paths passes near a 12 nm gold particle (figure 4), the phase-shift difference can be as large as $|\chi_1 - \chi_2| \sim 3^\circ$, which could be resolved in an electron holography setup. Additionally, we conclude that signatures of vacuum fluctuations should also be observed by monitoring the angular distribution of electrons after such interaction (e.g., in the Fourier plane of an electron microscope; see figures 2(b) and 3(c)). However, the electron deflections involved in such type of diffraction experiment could be overshadowed by very-low-energy inelastic contributions associated with Johnson noise [53, 63, 64], so the previously noted two-path holography experiment appears to be a more plausible solution to measure the quantum vacuum phase shift. It is our hope that the present work

contributes to clarify the role of vacuum fluctuations in macroscopic QED and supports the fact that an experimental verification is feasible using state-of-art electron microscopes. Considering the strong effect induced on the electron wave function by the quantum vacuum phase, we anticipate further efforts oriented toward the engineering of structures capable of tailoring vacuum fluctuations as a novel route to design free-electron phase plates. Additionally, this effort can lead to optimized strategies for electron microscope imaging: indeed, from the holography configuration discussed in section 2.2, taking path 2 to be far from both the sample and path 1, we have an interference term

$$\langle \hat{S}_2^\dagger \hat{S}_1 \rangle_T = \exp \left\{ \frac{-2ie^2}{\hbar} \int_0^\infty d\omega \int_{-\infty}^\infty dz \int_{-\infty}^\infty dz' \cos \left[\frac{\omega}{v} (z - z') \right] G_{z,z}^s(\mathbf{R}_1, z, \mathbf{R}_1, z', \omega) \right\}$$


at $T = 0$, clearly showing that the imaginary part of the Green tensor produces a depletion of the signal, while possibly creating excitations in the sample, whereas the real part determines the phase shift under discussion; for practical purposes in electron microscopy, it is useful to reduce the former (i.e., limit sample damage) while increasing the latter (i.e., enhance phase contrast), a task that leads to a problem of optimization in the present formalism. Our results for small noble-metal spheres (figure 2) already indicate that measurement of the quantum phase can be advantageous compared with bright-field imaging to avoid sample damage.

Acknowledgments

We thank Claus Ropers for helpful and enjoyable discussions. This work has been supported in part by ERC (Advanced Grant 789104-eNANO), the Spanish MINECO (MAT2017-88492-R and SEV2015-0522), the Catalan CERCA Program, Fundació Privada Cellex, and Fundació Mir-Puig. VDG acknowledges support from the EU (Skłodowska-Curie Grant 713729).

ORCID iDs

Valerio Di Giulio  <https://orcid.org/0000-0002-0948-4625>

F Javier García de Abajo  <https://orcid.org/0000-0002-4970-4565>

References

- [1] Verbeeck J, Tian H and Schattschneider P 2010 Production and application of electron vortex beams *Nature* **467** 301–4
- [2] Verbeeck J, Béché A, Müller-Caspary K, Guzzinati G, Luong M A and Den Hertog M 2018 Demonstration of a 2×2 programmable phase plate for electrons *Ultramicroscopy* **190** 58–65
- [3] Kapitza P L and Dirac P A M 1933 The reflection of electrons from standing light waves *Math. Proc. Camb. Phil. Soc.* **29** 297–300
- [4] Freimund D L, Aflatooni K and Batelaan H 2001 Observation of the Kapitza–Dirac effect *Nature* **413** 142–3
- [5] Vanacore G M *et al* 2019 Ultrafast generation and control of an electron vortex beam via chiral plasmonic near fields *Nat. Mater.* **18** 573–9
- [6] Konečná A and García de Abajo F J 2020 Electron beam aberration correction using optical near fields *Phys. Rev. Lett.* **125** 030801
- [7] Ford L H 1993 Electromagnetic vacuum fluctuations and electron coherence *Phys. Rev. D* **47** 5571–80
- [8] Aharonov Y and Bohm D 1959 Significance of electromagnetic potentials in the quantum theory *Phys. Rev.* **115** 485–91
- [9] Hsiang J-T and Lee D-S 2006 Influence on electron coherence from quantum electromagnetic fields in the presence of conducting plates *Phys. Rev. D* **73** 065022
- [10] Yoshioka H 1957 Effect of inelastic waves on electron diffraction *J. Phys. Soc. Jpn.* **12** 618–28
- [11] Rez P 1978 Virtual inelastic scattering in high-energy electron diffraction *Acta Crystallogr. A* **34** 48–51
- [12] Dung H T, Knöll L and Welsch D-G 1998 Three-dimensional quantization of the electromagnetic field in dispersive and absorbing inhomogeneous dielectrics *Phys. Rev. A* **57** 3931–42
- [13] Buhmann S Y 2012 *Dispersion Forces I. Macroscopic Quantum Electrodynamics and Ground-State Casimir, Casimir-Polder and van der Waals Forces* (Berlin: Springer)
- [14] Itzykson C and Zuber J B 2012 *Quantum Field Theory* (New York: Dover Publications)
- [15] Breuer H P and Petruccione F 2002 *The Theory of Open Quantum Systems* (Oxford: Oxford University Press)
- [16] Levinson Y 2005 Decoherence of electron beams by electromagnetic field fluctuations *J. Phys. A: Math. Gen.* **37** 3003–17
- [17] Howie A 2010 Mechanisms of decoherence in electron microscopy *Ultramicroscopy* **111** 761–7
- [18] Scheel S and Buhmann S Y 2012 Path decoherence of charged and neutral particles near surfaces *Phys. Rev. A* **85** 030101
- [19] Peter S and Hasselbach F 2007 Measurement of decoherence of electron waves and visualization of the quantum-classical transition *Phys. Rev. Lett.* **98** 200402
- [20] Beierle P J, Zhang L and Batelaan H 2018 Experimental test of decoherence theory using electron matter waves *New J. Phys.* **20** 113030
- [21] Kerker N, Röpke R, Steinert L M, Pooch A and Stibor A 2020 Quantum decoherence by coulomb interaction *New J. Phys.* **22** 063039
- [22] Howie A and Stern R M 1972 The optical potential in electron diffraction *Z. Naturforsch. A* **27** 382–9
- [23] Dederichs P H 1972 Dynamical diffraction theory by optical potential methods *Solid State Phys.* **27** 135–236
- [24] García de Abajo F J 2010 Optical excitations in electron microscopy *Rev. Mod. Phys.* **82** 209–75
- [25] Kreibig U and Vollmer M 1995 *Optical Properties of Metal Clusters* (Berlin: Springer)

- [26] García de Abajo F J 2008 Nonlocal effects in the plasmons of strongly interacting nanoparticles, dimers, and waveguides *J. Phys. Chem. C* **112** 17983–7
- [27] Cox J D and García de Abajo F J 2020 Nonlinear interactions between free electrons and nanographenes *Nano Lett.* **20** 4792–800
- [28] Rodríguez Echarri A, Skjølstrup E J H, Pedersen T G and García de Abajo F J 2020 Theory of electron energy-loss spectroscopy in atomically thin metallic films *Phys. Rev. Res.* **2** 023096
- [29] Liebsch A 1993 Surface-plasmon dispersion and size dependence of mie resonance: silver versus simple metals *Phys. Rev. B* **48** 11317–28
- [30] Liebsch A 1993 Surface plasmon dispersion of ag *Phys. Rev. Lett.* **71** 145–8
- [31] Hedin L, Lundqvist S and Ehrenreich H 1970 Effects of electron-electron and electron-phonon interactions on the one-electron states of solids *Solid State Physics (Solid State Physics, vol 23)* ed D Turnbull, F Seitz and H Ehrenreich (New York: Academic) pp 1–181
- [32] Bloch F 1933 Bremsvermögen von atomen mit mehreren elektronen *Z. Phys.* **81** 363–76
- [33] Mortensen N A, Raza S, Wubs M, Søndergaard T and Bozhevolnyi S I 2014 A generalized non-local optical response theory for plasmonic nanostructures *Nat. Commun.* **5** 3809
- [34] David C and García de Abajo F J 2014 Surface plasmon dependence on the electron density profile at metal surfaces *ACS Nano* **8** 9558–66
- [35] Ritchie R H 1957 Plasma losses by fast electrons in thin films *Phys. Rev.* **106** 874–81
- [36] Ritchie R H and Marusak A L 1966 The surface plasmon dispersion relation for an electron gas *Surf. Sci.* **4** 234–40
- [37] Feibelman P J 1982 Surface electromagnetic fields *Prog. Surf. Sci.* **12** 287–407
- [38] Yang Y *et al* 2019 A general theoretical and experimental framework for nanoscale electromagnetism *Nature* **576** 248–52
- [39] Buhmann S Y, Butcher D T and Scheel S 2012 Macroscopic quantum electrodynamics in nonlocal and nonreciprocal media *New J. Phys.* **14** 083034
- [40] W Milonni P 1994 *The Quantum Vacuum: An Introduction to Quantum Electrodynamics* (San Diego, CA: Academic)
- [41] Di Giulio V, Kociak M and García de Abajo F J 2019 Probing quantum optical excitations with fast electrons *Optica* **6** 1524–34
- [42] Park S T and Zewail A H 2012 Relativistic effects in photon-induced near field electron microscopy *J. Phys. Chem. A* **116** 11128–33
- [43] Glauber R J and Lewenstein M 1991 Quantum optics of dielectric media *Phys. Rev. A* **43** 467–91
- [44] Franke S, Hughes S, Dezfouli M K, Kristensen P T, Busch K, Knorr A and Richter M 2019 Quantization of quasinormal modes for open cavities and plasmonic cavity quantum electrodynamics *Phys. Rev. Lett.* **122** 213901
- [45] Messiah A 1966 *Quantum Mechanics* (New York: North-Holland)
- [46] Sakurai J J 1994 *Modern Quantum Mechanics* (Reading, MA: Addison-Wesley)
- [47] Carruthers P and Nieto M M 1965 Coherent states and the forced quantum oscillator *Am. J. Phys.* **33** 537–44
- [48] Glauber R J 1963 Coherent and incoherent states of the radiation field *Phys. Rev.* **131** 2766–88
- [49] Chaturvedi S, Sriram M S and Srinivasan V 1987 Berry's phase for coherent states *J. Phys. A: Math. Gen.* **20** L1071–5
- [50] Abrikosov A A, Gor'kov L P and Dzyaloshinskii I Y 1965 *Quantum Field Theoretical Methods in Statistical Physics* (New York: Pergamon)
- [51] Johnson P B and Christy R W 1972 Optical constants of the noble metals *Phys. Rev. B* **6** 4370–9
- [52] Palik E D 1985 *Handbook of Optical Constants of Solids* (San Diego, CA: Academic)
- [53] Howie A 2019 Continued skirmishing on the wave-particle frontier *Ultramicroscopy* **203** 52–9
- [54] Gradshteyn I S and Ryzhik I M 2007 *Table of Integrals, Series, and Products* (London: Academic)
- [55] Barton G 1977 Quantum mechanics of charged particles near a plasma surface *J. Phys. A: Math. Gen.* **10** 601–12
- [56] Gonçalves P A D, Christensen T, Jauho N R A, Mortensen N A and Soljačić M M 2020 Plasmon-emitter interactions at the nanoscale *Nat. Commun.* **11** 366
- [57] Gonçalves P A D 2020 *Plasmonics and Light-Matter Interactions in Two-Dimensional Materials and in Metal Nanostructures: Classical and Quantum Considerations* (Cham: Springer)
- [58] Koppens F H L, Chang D E and García de Abajo F J 2011 Graphene plasmonics: a platform for strong light-matter interactions *Nano Lett.* **11** 3370–7
- [59] Gusynin V P, Sharapov S G and Carbotte J P 2009 On the universal ac optical background in graphene *New J. Phys.* **11** 095013
- [60] Yu R, Manjavacas A and García de Abajo F J 2017 Ultrafast radiative heat transfer *Nat. Commun.* **8** 2
- [61] Potapov P L, Lichte H, Verbeeck J and van Dyck D 2006 Experiments on inelastic electron holography *Ultramicroscopy* **106** 1012–8
- [62] Mandel L and Wolf E 1995 *Optical Coherence and Quantum Optics* (Cambridge: Cambridge University Press)
- [63] Uhlemann S, Müller H, Zach J and Haider M 2014 Thermal magnetic field noise: electron optics and decoherence *Ultramicroscopy* **151** 199–210
- [64] Howie A 2014 Addressing Coulomb's singularity, nanoparticle recoil and Johnson's noise *J. Phys.: Conf. Ser.* **522** 012001